Arch. Metall. Mater. **63** (2018), 2, 749-763

DOI: 10.24425/122401

R. SHASHANKA*,**#, D. CHAIRA**, B.E. KUMARA SWAMY***

EFFECT OF Y_2O_3 NANOPARTICLES ON CORROSION STUDY OF SPARK PLASMA SINTERED DUPLEX AND FERRITIC STAINLESS STEEL SAMPLES BY LINEAR SWEEP VOLTAMMETRIC METHOD

The microstructure and corrosion properties of spark plasma sintered yttria dispersed and yttria free duplex and ferritic stainless samples were studied. Spark plasma sintering (SPS) was carried out at 1000°C by applying 50 MPa pressure with holding time of 5 minutes. Linear sweep voltammetry (LSV) tests were employed to evaluate pitting corrosion resistance of the samples. Corrosion studies were carried out in 0.5, 1 and 2 M concentration of NaCl and H_2SO_4 solutions at different quiet time of 2, 4, 6, 8 and 10 seconds. Yttria dispersed stainless steel samples show more resistance to corrosion than yttria free stainless steel samples. Pitting potential decreases with increase in reaction time from 2 to 10 seconds. Similarly, as concentration of NaCl and H_2SO_4 increases from 0.5 M to 2 M the corrosion resistance decrements due to the availability of more Cl^- and SO_4^{2-} ions at higher concentration.

Keywords: Duplex stainless steel, pitting corrosion, spark plasma sintering, linear sweep voltammetry, ball milling

1. Introduction

Duplex and ferrite are the two important types of stainless steels. Duplex stainless steel show excellent corrosion resistant property, electrocatalytic property [1], good high-temperature tensile and creep strength. Hence it is used as corrosion resistant super heaters, re-heaters and high temperature boilers to improve their performances [2]. Whereas ferritic stainless steel has the properties of less stress corrosion, low thermal expansion, excellent high temperature oxidation resistance, high thermal conductivity, creep resistance and high yield strength [3]. Shashanka et al. [4] reported that, ferritic stainless steels are mainly used in refrigeration cabinets, benchwork, cold water tanks, chemical and food processing, water treatment plant, street furniture, electrical cabinets etc.

Powder metallurgy is one of the most effective methods to produce complex shaped materials and high productivity. Shankar et al. [5] reported that, powder metallurgy (P/M) components show relatively poor mechanical and corrosion properties when compared with wrought products and hence their applications are limited. Therefore, more research work is going on to improve the mechanical and corrosion properties of P/M products. The properties of P/M components can be improved by using advanced sintering techniques and by adding second phase particles as reported by German [6] and Mukherjee et al. [7,8].

Spark plasma sintering (SPS) is an advanced sintering technique that has attracted substantial interest for fabrication of poorly sinterable materials. The SPS process involves simultaneous application of load as well as heat on the materials to be sintered. SPS is a new method meant for consolidation of nano structured materials with hindered grain growth, efficient shrinkage in less time and cleaner grain boundaries for effective interface formation [9]. This technique utilizes high temperature spark plasma generated by discharging exactly at the gaps of powder particles with an on-off electrical current [10]. At the initial stage of SPS process, the generated spark plasma induces neck formation and thermal diffusion process on the particles to be sintered. Electric field formed by DC current can also facilitates thermal diffusion process. Therefore, SPS process involves densification of poorly sinterable materials at a very short interval of time and at low temperature when compared with conventional sintering process as reported by Tokita [11], Omori [12] and Kim et al. [13]. The addition of dispersoids can enhance the corrosion resistance and mechanical properties of P/M components [14]. The oxygen active elements impart more strength to interfacial bonding and forms stronger oxide layer to prevent further corrosion. Yttria is one of the oxygen active elements which enhance the oxide adherence [15-18]. Hence, we prepared yttria dispersed duplex and ferritic stainless steel samples by SPS method. The addition of yttria increases the corrosion resistance of stainless steel and it rapidly forms a protective chromium oxide layer on the surface to prevent further corrosion.

Shankar et al. [5] studied pitting corrosion resistance of yttria dispersed stainless steel by cyclic polarization experiments

* PRESIDENCY UNIVERSITY, DEPARTMENT OF CHEMISTRY, SCHOOL OF ENGINEERING, BENGALURU-560064, INDIA.
** NATIONAL INSTITUTE OF TECHNOLOGY, DEPARTMENT OF METALLURGICAL AND MATERIALS ENGINEERING, ROURKELA-769008, INDIA
*** KUVEMPU UNIVERSITY, DEPARTMENT OF P.G .STUDIES AND RESEARCH IN INDUSTRIAL CHEMISTRY, JNANA SAHYADRI, SHANKARAGHATTA 577451, SHIMOGA, KARNATAKA, INDIA.
# Corresponding author: shashankaic@gmail.com

in 3.56 wt. % NaCl solution. They concluded that the addition of Y_2O_3 did not affect the pitting corrosion resistance. The corrosion resistance values obtained for Y_2O_3 dispersed stainless steels are comparable with the wrought stainless steel samples. The pitting resistance of the samples sintered at 1250°C is superior to the samples sintered at 1400°C. Lal and Upadhyaya [19,20] studied the effect of Y_2O_3 addition on sintering behaviour of austenitic stainless steel. They reported that 4wt. % addition of yttria increases both sintered density and corrosion resistance, which was attributed to the interaction of Cr_2O_3 with dispersoids. Ningshen et al. [21] reported the corrosion resistance of 12% and 15% chromium oxide dispersion strengthened (ODS) steels in 3 M and 9 M HNO_3 respectively. They observed that 12% chromium ODS steel exhibit high corrosion rate than 15% chromium ODS steel at both 3 M and 9 M HNO_3 concentrations. The pitting corrosion potential value of both the types of ODS steels shift close to the trans-passive region due to the increase in HNO_3 concentration. Balaji et al. [14] studied the corrosion resistance of yttria aluminium garnet (YAG) dispersed austenitic stainless steel sintered at 1200 and 1400°C respectively. Different concentrations (1.0, 2.5 and 7.5 wt.%) of the second phase YAG was added to austenitic stainless steel. The corrosion studies were carried out in 0.1N H_2SO_4 using potentiodynamic polarization. They reported that addition of YAG does not increase corrosion rate appreciably but super-solidus sintering show higher corrosion resistance than solid-state sintering.

Most of the corrosion studies were carried out using electrochemical methods such as impedance spectroscopy [22], polarographic methods [23], cyclic voltammetry [24] etc. But no literature is available so far according to author's best knowledge on the corrosion study of yttria dispersed and yttria free duplex and ferritic stainless steel samples by Linear sweep voltammetry (LSV) method. LSV is an important electrochemical technique involves solid electrode, fixed potential and fast scan rate. The slope of the ramp has units of volts per unit time and is generally called as scan rate of the experiment [25,26]. The results obtained by LSV method in the present study are comparable with the results obtained by impedance, polarographic methods as reported by Jian Chen et al. [22] and Li et al. [23]. Time required in determining the pitting potential of stainless steel is of the order of few seconds and there is no need to keep stainless steel samples in NaCl or other electrolytes for many months. Cyclic voltammetry and LSV techniques are mainly used to determine pharmaceutical drugs, metal ions and many more environmental applications [27-30].

2. Experimental

2.1. Consolidation of duplex and ferritic stainless steel by SPS

Duplex and ferritic stainless steel powders were prepared by wet (toluene) milling of elemental powders of compositions Fe-18Cr-13Ni (wt. %) and Fe-17Cr-1Ni (wt. %) respectively in a specially built dual-drive planetary mill for 10 hours. The detail study of duplex and ferritic stainless steel powder preparation was explained by Shashanka et al. [31-35]. The powders were mixed separately with 1wt. % nano structured Y_2O_3 powder particles by turbula shaker mixture (TURBULA® T2F, Willy A. Bachofen AG Maschinenfabrik, Switzerland) for 3hours [36-38]. The average particle size of as received Y_2O_3 nanoparticles are found to be 40 nm [37]. Yttria dispersed and yttria free duplex and ferritic stainless steel powder samples were consolidated by SPS method. SPS **(**SCM 1050, Sumitomo Coal Mining Co, Ltd Japan) was carried out at 1000°C under a pressure of 50 MPa for 5 minutes in a graphite die of 20 mm diameter. The consolidated stainless steel samples were characterized by X-ray diffraction (XRD) in a Philips PANalytical diffractometer using filtered Cu Kα-radiation ($\lambda = 0.1542$ nm). Field emission scanning electron microscopy (FESEM) was carried out in FEI NANO NOVA 450 to study the morphology of sintered stainless steel.

2.2. Corrosion study by LSV method

The corrosion studies were carried out in a well-established three electrode electrochemical cell using electrochemical work station CHI-660c model by LSV method. Potential scans were collected in a freely aerated NaCl and H_2SO_4 solutions at room temperature. The experiments were carried out in an electrochemical cell containing Ag/AgCl saturated KCl as reference electrode, stainless steel samples as working electrode (20 mm diameter) and platinum counter electrode. Different concentrations of NaCl and H_2SO_4 solutions were employed to study the effect of electrolyte concentration on corrosion. The microstructure of consolidated stainless steel samples were investigated by Carl Zeiss optical microscope and phase fraction of corroded duplex and ferritic stainless steels were calculated by using Axio Vision Release 4.8.2 SP3 (08-2013) software.

3. Results and discussion

3.1. Characterization of SPS consolidated stainless steel samples

3.1.1. Phase analysis

The XRD spectra of yttria dispersed duplex and ferritic stainless steel samples are shown in Fig. 1a & 1b respectively. XRD spectra of consolidated yttria dispersed stainless steel samples exhibit sharp crystalline and broad diffraction peaks of ferrite, austenite phases along with traces of yttria peaks. No trace of diffraction peaks like sigma phase; carbides or nitrides precipitations of secondary phases can be seen in both the stainless steel samples. The broad but yet crystalline peaks in both the samples are due to the diffusion phenomenon as well as reduced grain growth during SPS. Fig. 1a show dominant austenite peaks due to its stability at higher temperatures. At a temperature of

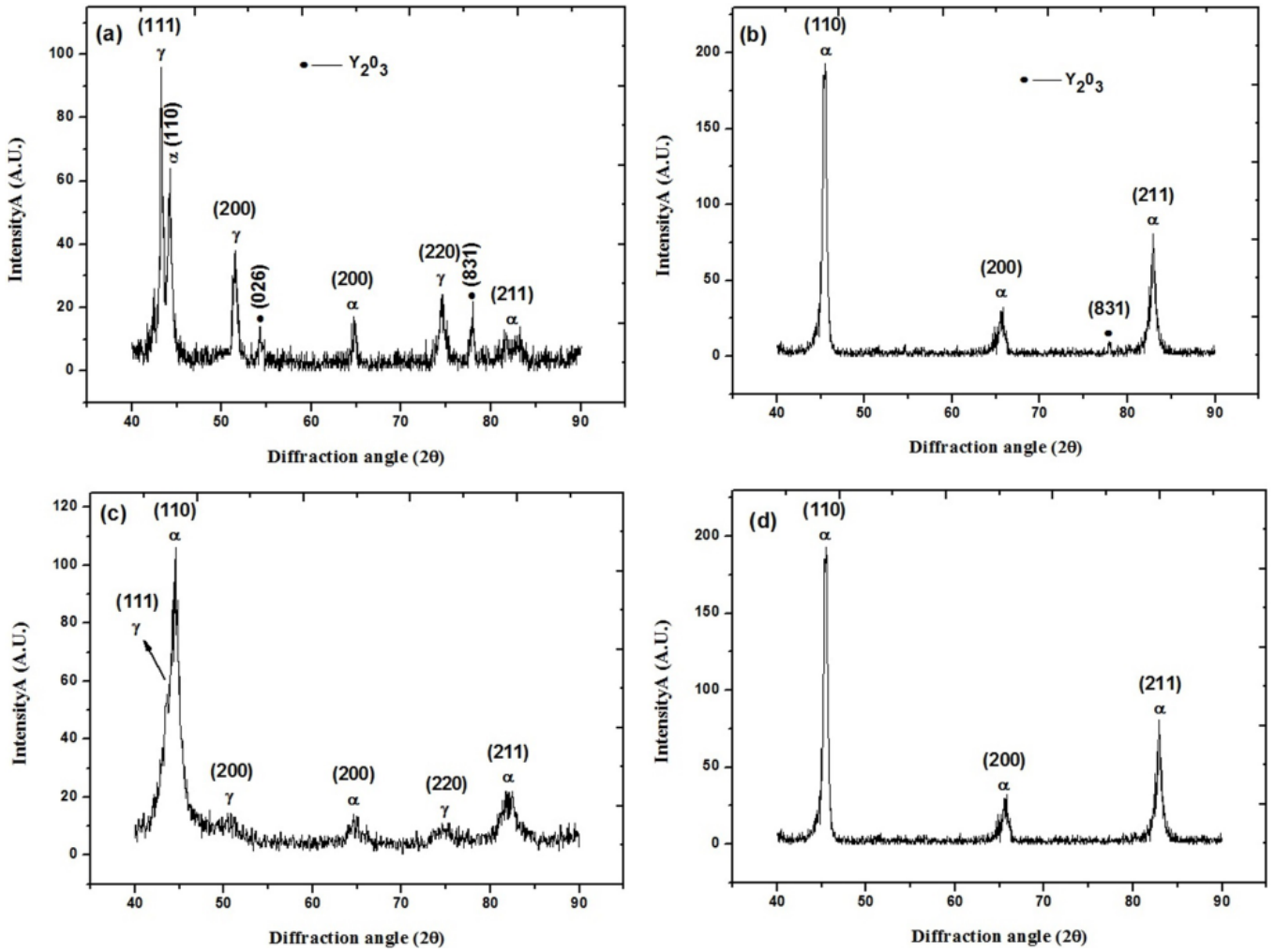

Fig. 1. XRD spectra of SPS consolidated (a) Yttria dispersed duplex stainless steel (b) Yttria dispersed ferritic stainless steel (c) duplex stainless steel (d) ferritic stainless steel

723°C, phase transformation from α-Fe to γ-Fe begins. Yttria dispersed ferritic stainless steel show only sharp dominant ferrite peaks. XRD spectra of yttria free duplex and ferritic stainless steel samples are shown in Fig. 1c and 1d respectively. Both the samples show sharp crystalline austenite and ferrite diffraction peaks without any secondary phases. Yttria dispersed duplex stainless steel show more dominant austenite peaks than yttria free duplex stainless steel. The effect of yttria during austenitic phase transformation is unknown. Hence, more research work has to be done regarding the mechanism of yttria during austenitic stabilization.

3.1.2. Microstructure study

FESEM micrographs of SPS consolidated yttria dispersed and yttria free duplex and ferritic stainless steel samples are presented in Fig. 2a-d respectively. From the figures it is clear that all the consolidated stainless steel samples are dense and almost free from pores. Fig. 2a and 2b depicts the dispersed yttria nano particles in duplex as well as ferritic stainless steel samples. The size of the yttria is measured from the FESEM images and it is found to be around 80 to 90 nm. Fig. 3a-c and 3d show EDX and the elemental analysis of duplex and ferritic stainless steel samples. It is evident from EDX that elemental composition of consolidated stainless steel samples are very close to the nominal composition of initial stainless steel powder samples. From elemental mapping it is clear that all the elements present in stainless steel are uniformly distributed.

3.2. Corrosion study of yttria dispersed and yttria free stainless steel samples by LSV

3.2.1. Different concentration of NaCl electrolyte solution

Fig. 4 depicts the mechanism of corrosion process in stainless steel. In the present work we studied the effect of reaction time (quiet time) and the effect of different concentration of NaCl electrolyte on pitting corrosion. The NaCl electrolytes of concentrations 0.5, 1 and 2 M were prepared in double distilled water and used to study corrosion. All the consolidated stainless steel samples were polished to 4/0 grade finish and cleaned with dis-

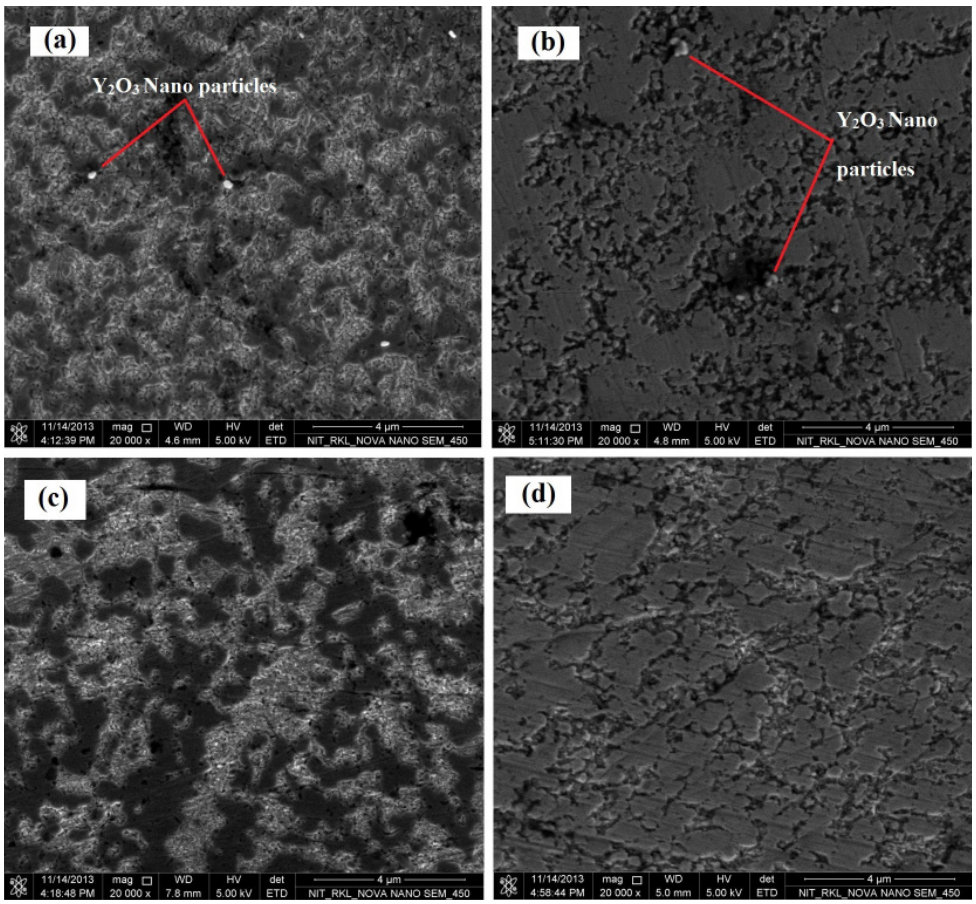

Fig. 2. FESEM images of SPS consolidated (a) Yttria dispersed duplex stainless steel (b) Yttria dispersed ferritic stainless steel (c) duplex stainless steel (d) ferritic stainless steel

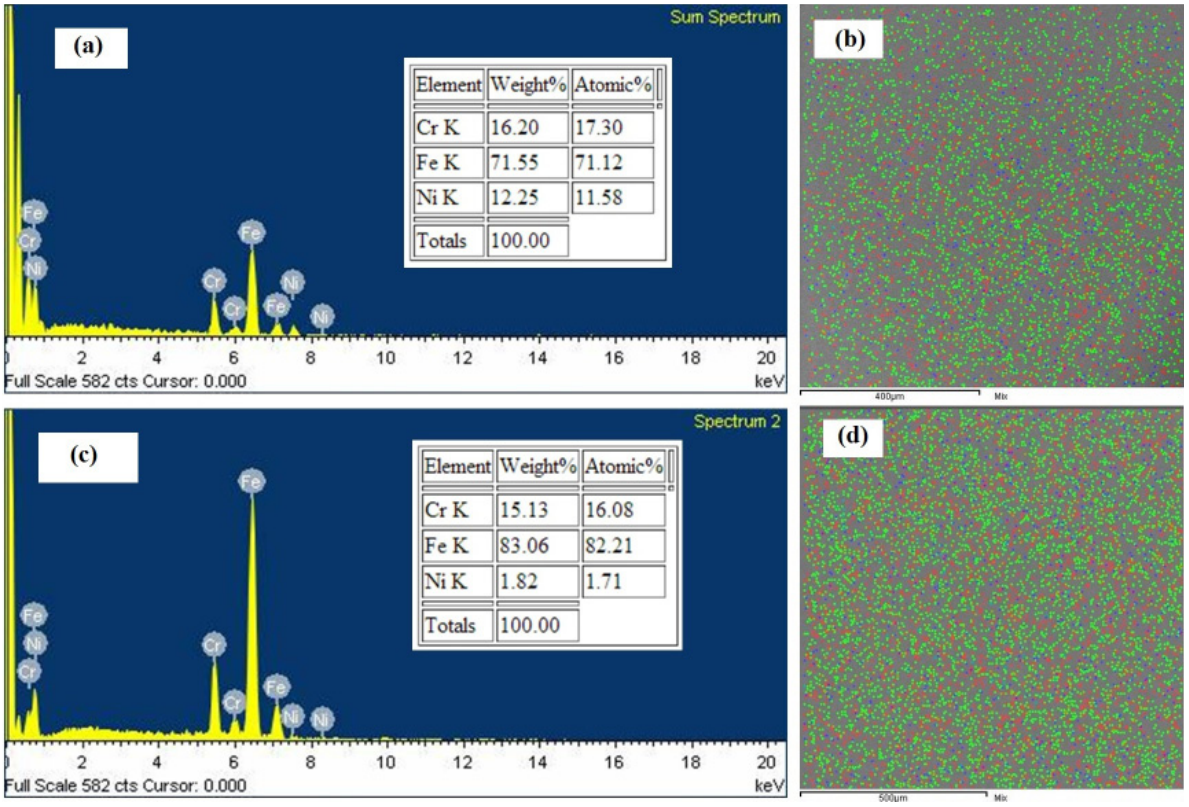

Fig. 3. EDX and elemental mapping of SPS consolidated (a)(b) Duplex stainless steel, (c)(d) Ferritic stainless steel respectively (In elemental mapping, Green – Fe, Red – Cr, Blue – Ni)

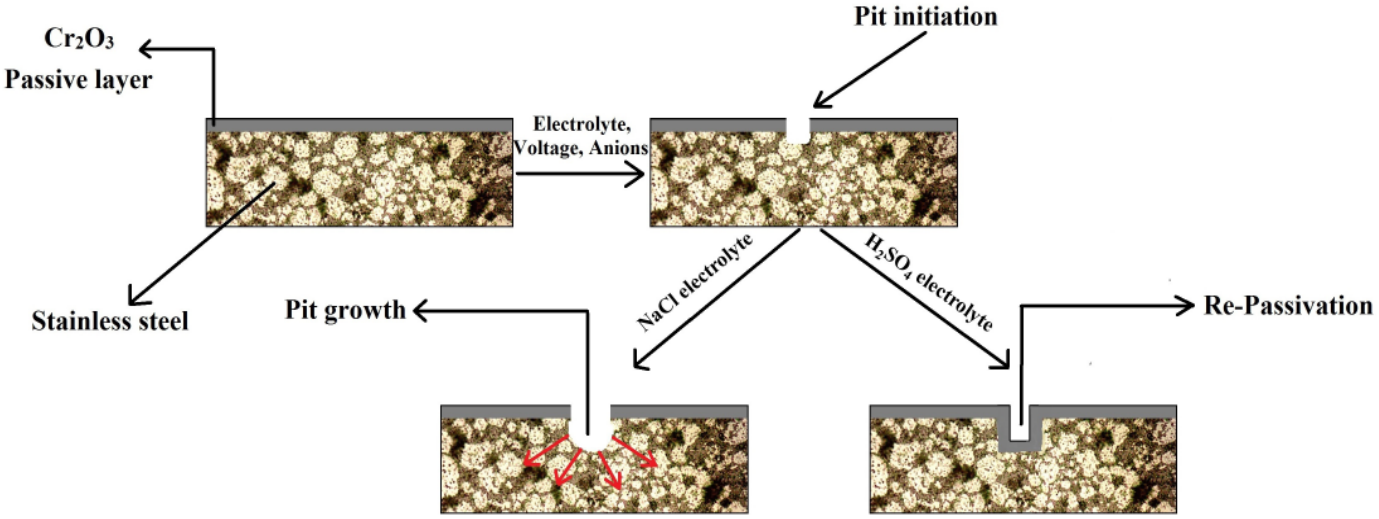

Fig. 4. Mechanism of corrosion in stainless steel samples

tilled water before the experiment in each case. The stainless steel [working electrode] whose corrosion properties to be studied was kept inside the electrochemical cell containing NaCl electrolyte, counter electrode and reference electrode. LSV was performed at a sweeping potential from 0.9 to 0 V (adjusted according to the pitting potential) with different quiet time from 2, 4, 6, 8 and 10 seconds. A curve of current and potential is obtained for each individual quiet time at constant concentration. Fig. 5a-c and 5d represent the LSV curve of current versus voltage variation of yttria dispersed and yttria free duplex and ferritic stainless steel samples at 0.5 M NaCl electrolyte at different quiet time. As the potential sweeps from 0.9 to 0 V the sharp increase in current takes place at a particular potential and that potential is called as pitting potential (E_P). The sharp increase in current is due to the availability of more electrons after passing through Cr_2O_3 layer. This results in pitting and it grows if the metal is unprotected. Some of the reactions responsible for corrosion in stainless steel at NaCl electrolytes are shown below.

Anodic reaction:

$Fe \rightarrow Fe^{2+} + 2e^{-}$ (Dissolution of Iron)

$Fe^{2+} + 2H_2O \rightarrow FeOH^{+} + H_3O^{+}$

Formation of $FeOH^{+}$ is mainly responsible for the sudden increase in current due to the dissolution of Fe metal.

Cathodic reaction:

$O_2 + 2H_2O + 4e^{-} \rightarrow 4OH^{-}$

Main reaction:

$Fe^{2+} + 2Cl^{-} \rightarrow FeCl_2$

$FeCl_2 + 2H_2O \rightarrow Fe(OH)_2 + 2HCl$

Formation of $Fe(OH)_2$ decreases the pH of the electrolyte inside a pit from 6 to 2, which induces further corrosion process.

The pitting corrosion process is evidenced by the LSV measurement method by sudden and drastic increase in pitting current (I_P) as shown in the Fig. 5. E_P values of yttria duplex and ferritic stainless steel samples are found to be 1.45 V and 0.64 V respectively. Similarly yttria free duplex and ferritic stainless steel samples have E_P value of 0.63 V and 0.57 V respectively. Yttria dispersed stainless steel samples show more E_P value than yttria free samples due to the presence of oxygen active yttria, which imparts more strength to interfacial bonding and forms strong oxide layer. Hence, more potential is required to break the oxide layer. Therefore yttria dispersed stainless steel samples show maximum pitting potential. The higher the pitting potential the better the corrosion resistance is [39]. The effect of current density on E_P for all the four stainless steel samples was studied successfully. The current density was calculated using equation (1) as follows.

$$J = \frac{I}{A} \tag{1}$$

Where, J is the current density, I is the pitting current and A is the area of working electrode used. Fig. 5e-g and 5h show the effect of current density on E_P in the case of yttria dispersed and yttria free duplex and ferritic stainless steel respectively. As the current density decreases both E_P and I_P increases. Similarly, whole experimental procedure was repeated for the same stainless steel samples at 1 M and 2 M NaCl concentrations, respectively. Fig. 6a-d and Fig. 6e-h show the current vs. voltage graphs and current density vs. E_P curves of yttria dispersed and yttria free duplex and ferritic stainless steel samples at 1 M NaCl concentration. E_P values of yttria dispersed duplex and ferritic stainless steel samples at 1 M NaCl are 0.67 V and 0.43 V respectively and for yttria free duplex and ferritic stainless steel samples have E_P value of 0.57 V and 0.19 V respectively. Similarly, Fig. 7a-d and Fig. 7e-h show the current versus voltage graphs and current density versus E_P curves of yttria dispersed and yttria free duplex and ferritic stainless steel samples at 2M NaCl concentration. Yttria dispersed duplex and ferritic stainless steel samples possess E_P value of 0.63V and 0.43V respectively. Similarly for yttria free duplex and ferritic stainless steel samples have E_P value of 0.24 V and 0.18 V respectively. From the graphs it is clear that as the concentration of NaCl electrolyte increases from 0.5 to 2 M then pitting potential for all the four stainless steel samples decreases due to the accelerated rate of corrosion reactions at higher concentrations.

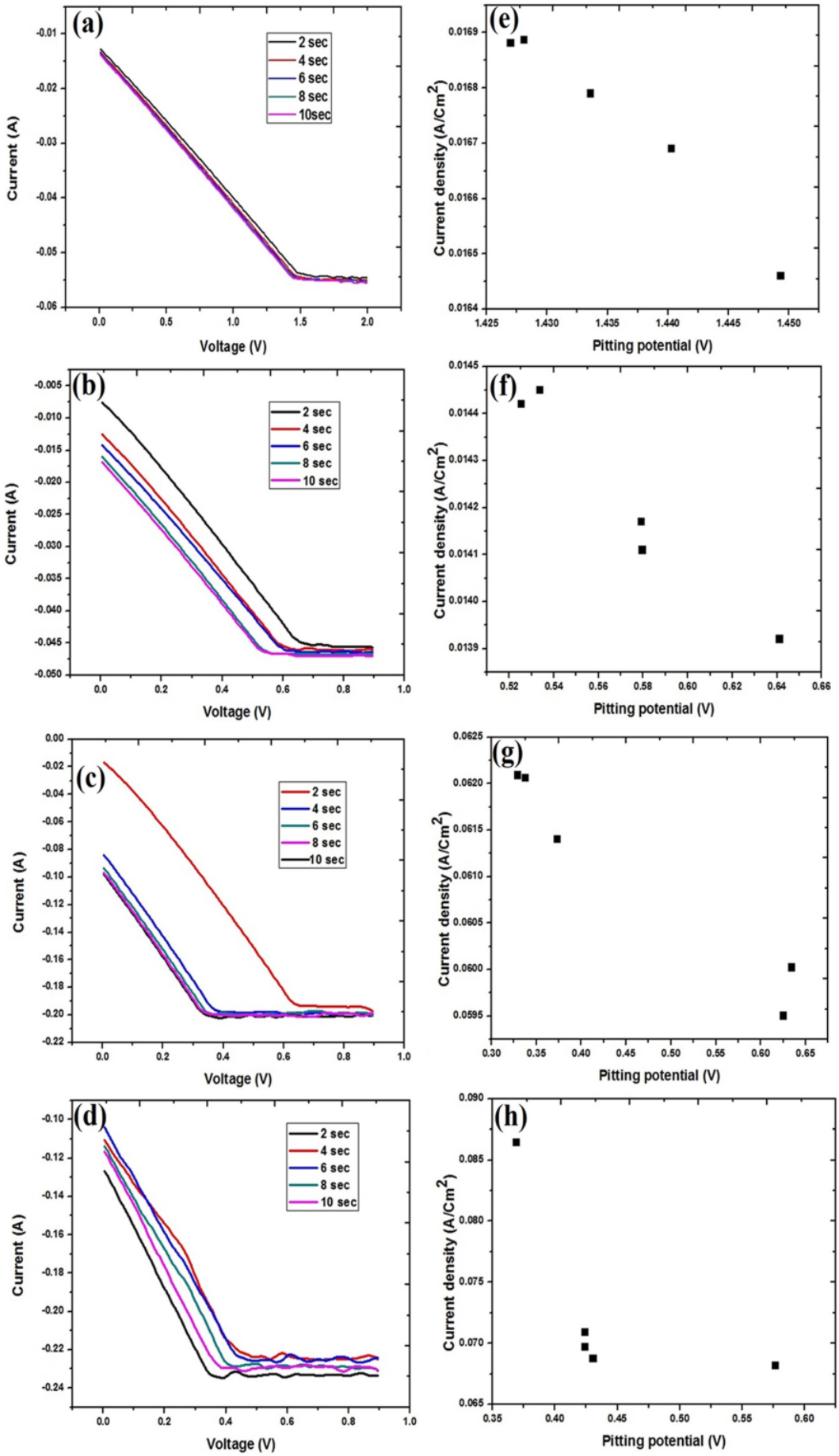

Fig. 5. Potentiometric curves and current density vs. pitting potential graphs of (a)(e) Yttria dispersed duplex stainless steel, (b)(f) Yttria dispersed ferritic stainless steel, (c)(g) duplex stainless steel, (d)(h) ferritic stainless steel respectively at 0.5 M NaCl solution

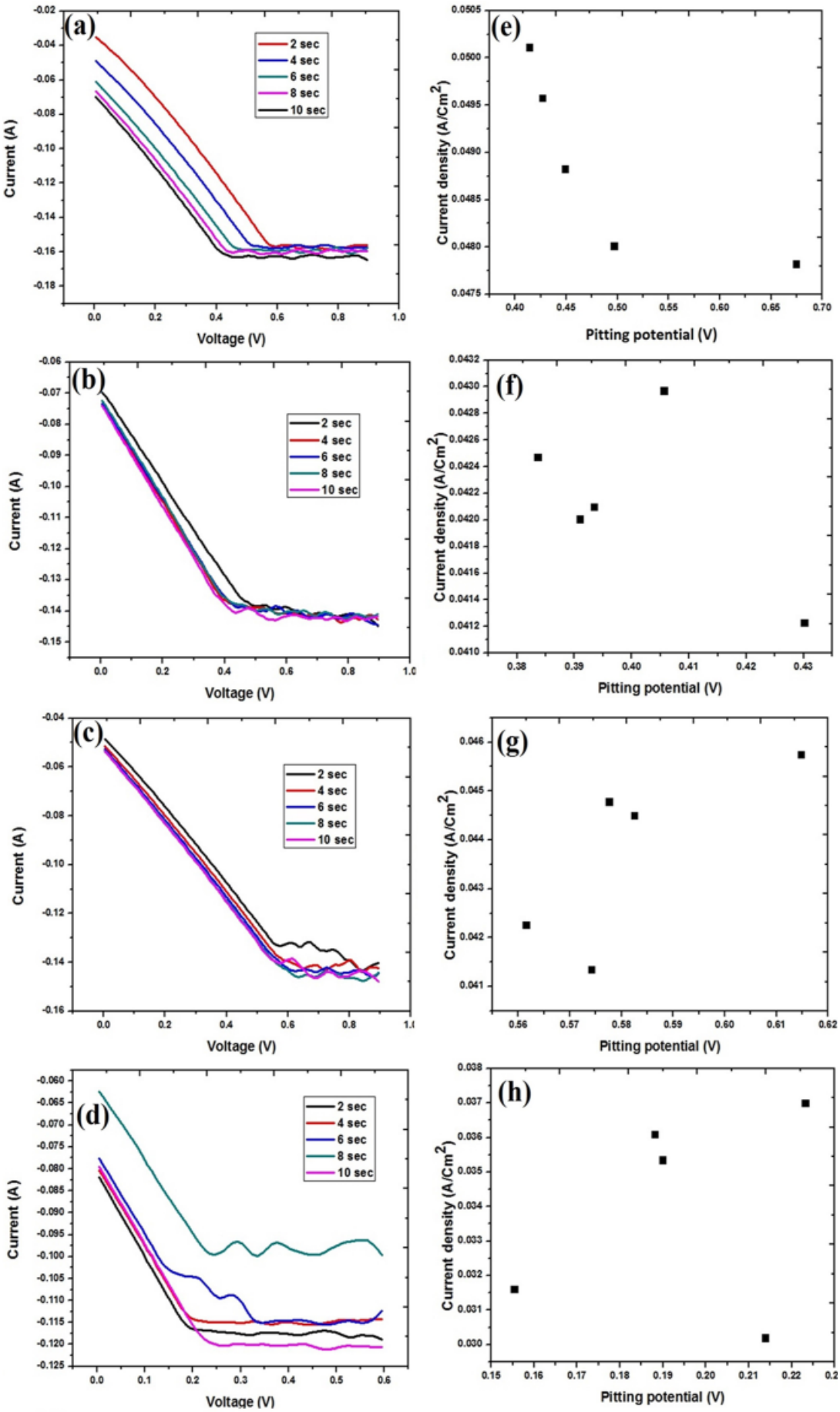

Fig. 6. Potentiometric curves and current density vs. pitting potential graphs of (a)(e) Yttria dispersed duplex stainless steel, (b)(f) Yttria dispersed ferritic stainless steel, (c)(g) duplex stainless steel, (d)(h) ferritic stainless steel respectively at 1 M NaCl solution

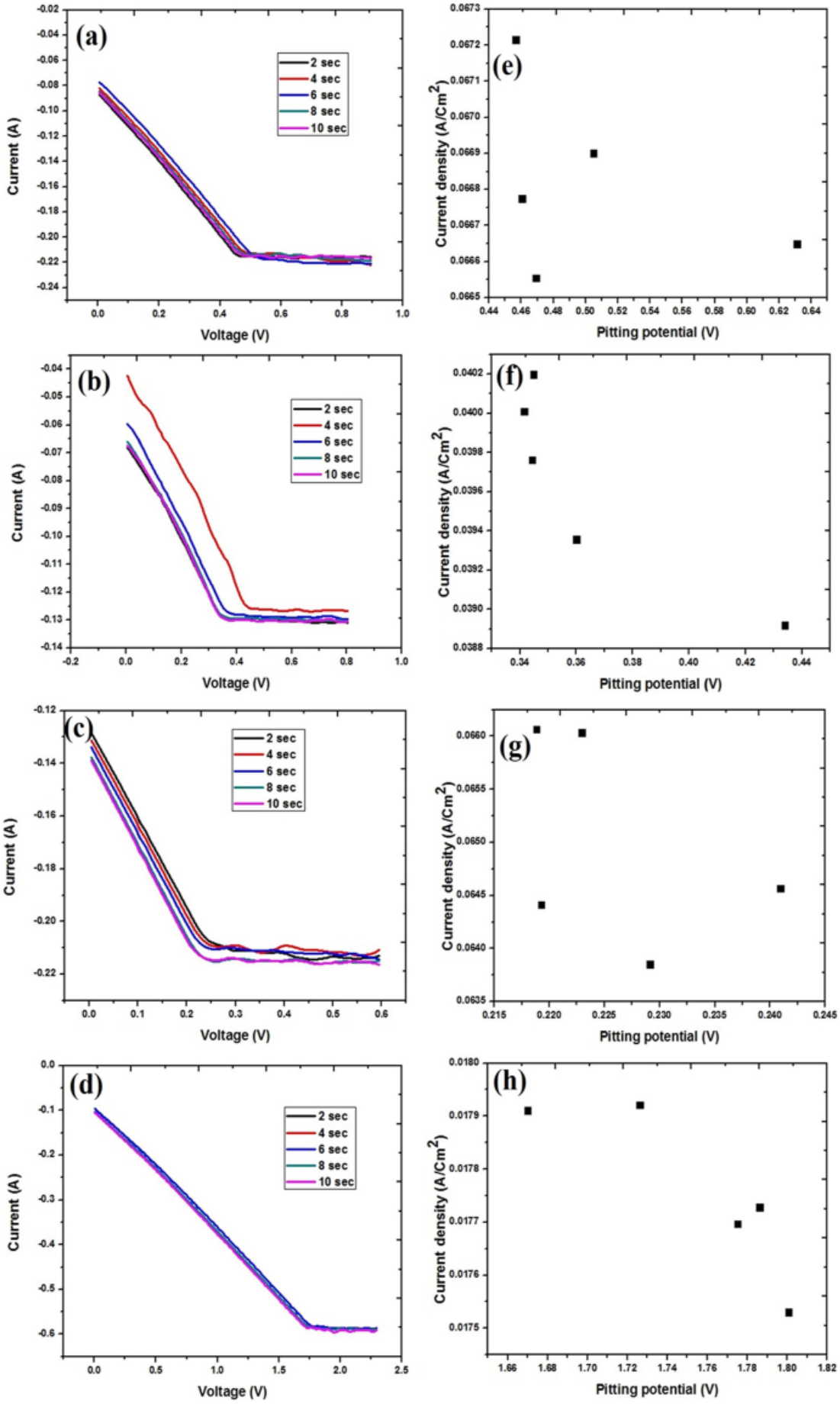

Fig. 7. Potentiometric curves and current density vs. pitting potential graphs of (a)(e) Yttria dispersed duplex stainless steel, (b)(f) Yttria dispersed ferritic stainless steel, (c)(g) duplex stainless steel, (d)(h) ferritic stainless steel respectively at 2 M NaCl solution

3.2.2. Different concentration of H_2SO_4 electrolyte solution

The corrosion studies were carried out in a same electrochemical experimental set up and same condition as the corrosion studies conducted in NaCl electrolyte. But here NaCl electrolyte was replaced by H_2SO_4 electrolyte to study the effect of acid electrolyte on corrosion of stainless steel samples. The H_2SO_4 electrolytes of 0.5, 1 and 2 M concentrations were prepared in double distilled water and used for the corrosion study of yttria dispersed and yttria free duplex and ferritic stainless steel samples.

A sweeping potential of 0.6 to 0 V (adjusted according to the pitting potential) is applied in LSV with different quiet time of 2, 4, 6, 8 and 10 seconds. A voltammetric curve is obtained for each individual quiet time at particular constant concentration. LSV curve of current versus voltage variation in yttria dispersed and yttria free duplex and ferritic stainless steel samples at 0.5 M H_2SO_4 electrolyte after 2, 4, 6, 8 and 10 seconds are shown in Fig. 8a-c and 8d respectively. From the figures it is clear that there is a sharp and sudden increase in the current between the potential 0.6 to 0V. E_P values of yttria duplex and ferritic stainless steel samples are 0.30 V and 0.23 V respectively at 0.5M H_2SO_4 electrolyte. Similarly for yttria free duplex and ferritic stainless steel samples have E_P value of 0.18 V and 0.14 V respectively.

The mechanism of corrosion in H_2SO_4 and NaCl solutions are almost same for all the four SPS consolidated stainless steel samples. The only difference is extent of pitting, pitting potential and pitting current values. Pitting potential value obtained under H_2SO_4 electrolyte setup is comparatively low compared to the results obtained during NaCl electrolyte. Stainless steel samples undergo corrosion easily in presence of H_2SO_4 than NaCl electrolyte. Current density is calculated using equation (1) and successfully studied the effect of current density on E_P. Fig. 8e-g and 8h represent the effect of current density on E_P of yttria dispersed and yttria free duplex and ferritic stainless steel respectively. As the current density decreases the pitting potential of all the samples also decreases with increase in pitting current.

We successfully studied the effect of E_P at 1M and 2M H_2SO_4 concentrations by maintaining the same procedure as explained above. Fig. 9a-d and Fig. 9e-h show the current versus voltage graphs and current density versus E_P curves of yttria dispersed and yttria free duplex and ferritic stainless steel samples at 1M H_2SO_4 solution. E_P values of yttria dispersed duplex and ferritic stainless steel samples at 1 M H_2SO_4 are found to be 0.19 V and 0.15 V respectively. Similarly for yttria free duplex and ferritic stainless steel samples show E_P values of 0.17 V and 0.14 V respectively. Fig. 10a-d and Fig. 10e-h show the current versus voltage graphs and current density versus E_P curves of yttria dispersed and yttria free duplex and ferritic stainless steel samples at 2M H_2SO_4 solution. Yttria dispersed duplex and ferritic stainless steel samples possess E_P value of -0.080V and 0.067 V respectively. Similarly, for yttria free duplex and ferritic stainless steel samples have E_P value of 0.028 V and -0.013 V respectively. From the graphs it is clear that as the concentration of H_2SO_4 increases from 0.5 to 1 M both pitting potential and current density increases due to the following reactions,

Anodic reaction:

$$Fe \rightarrow Fe^{2+} + 2e^{-} \text{ (Dissolution of Iron)}$$

Cathodic reaction:

$$2H^{+} + 2e^{-} \rightarrow H_2$$

The main corrosion reaction gives the products iron sulphate and hydrogen gas as shown below.

Main reaction:

$$Fe + H_2SO_4 \rightarrow FeSO_4 + H_2$$

$FeSO_4$ forms a thin layer on the stainless steel surface and acts as a passive protective layer for corrosion. But the released hydrogen gas scrub off the $FeSO_4$ layer and causes corrosion [40]. In case of 0.5 and 1M H_2SO_4 electrolyte the formed protective $FeSO_4$ layer bounds strongly to the surface of stainless steel along with Cr_2O_3 layer and hence hydrogen gas liberated during these concentrations is not enough to break the oxide layer to form a pit and to initiate corrosion. Hence at 0.5 and 1 M H_2SO_4 solution, the corrosion studies concluded with higher E_P and maximum current density. But in case of 2 M H_2SO_4 solution, the hydrogen gas liberated is sufficient to scrub off the $FeSO_4$ layer at very low potential. As a result of this, all the four stainless steel samples show low pitting potential at 2 M H_2SO_4. The values of E_P and current density with different electrolytes were tabulated in Table 1.

4. Microstructural analysis of SPS consolidated stainless steel samples after corrosion study

Fig. 11 depicts the FESEM images of yttria dispersed and yttria free duplex and ferritic stainless steel samples. From FESEM images we can see the grey colour corrosion regions clearly in all the samples. Optical image analysis is carried out to study the microstructure of corroded yttria dispersed and yttria free duplex and ferritic stainless steel. All the four stainless steel samples are free from voids as they were consolidated by SPS at 1000°C. Fig. 12 and Fig. 13 show the microstructure and phase analysis of stainless steel after corrosion. The black coloured region is corroded region containing iron oxide. All the stainless steel samples are having black region in the microstructure confirming the occurrence of corrosion during electrochemical measurement. Microstructural analysis is conducted to those stainless steel samples whose corrosion studies were performed by LSV method at 2M H_2SO_4 solution. According to corrosion studies, the rate of corrosion is more in yttria free stainless steel samples than yttria dispersed samples and it is confirmed by micro structural analysis. Phase analysis was carried out to study the volume fraction of iron oxide present in stainless steel samples. The presence of iron oxide volume percentage is more in yttria free stainless steel samples than yttria dispersed samples and the values are tabulated in Table 1. The volume fraction of iron oxide phase is determined by Axio Vision Release software. In Fig. 13,

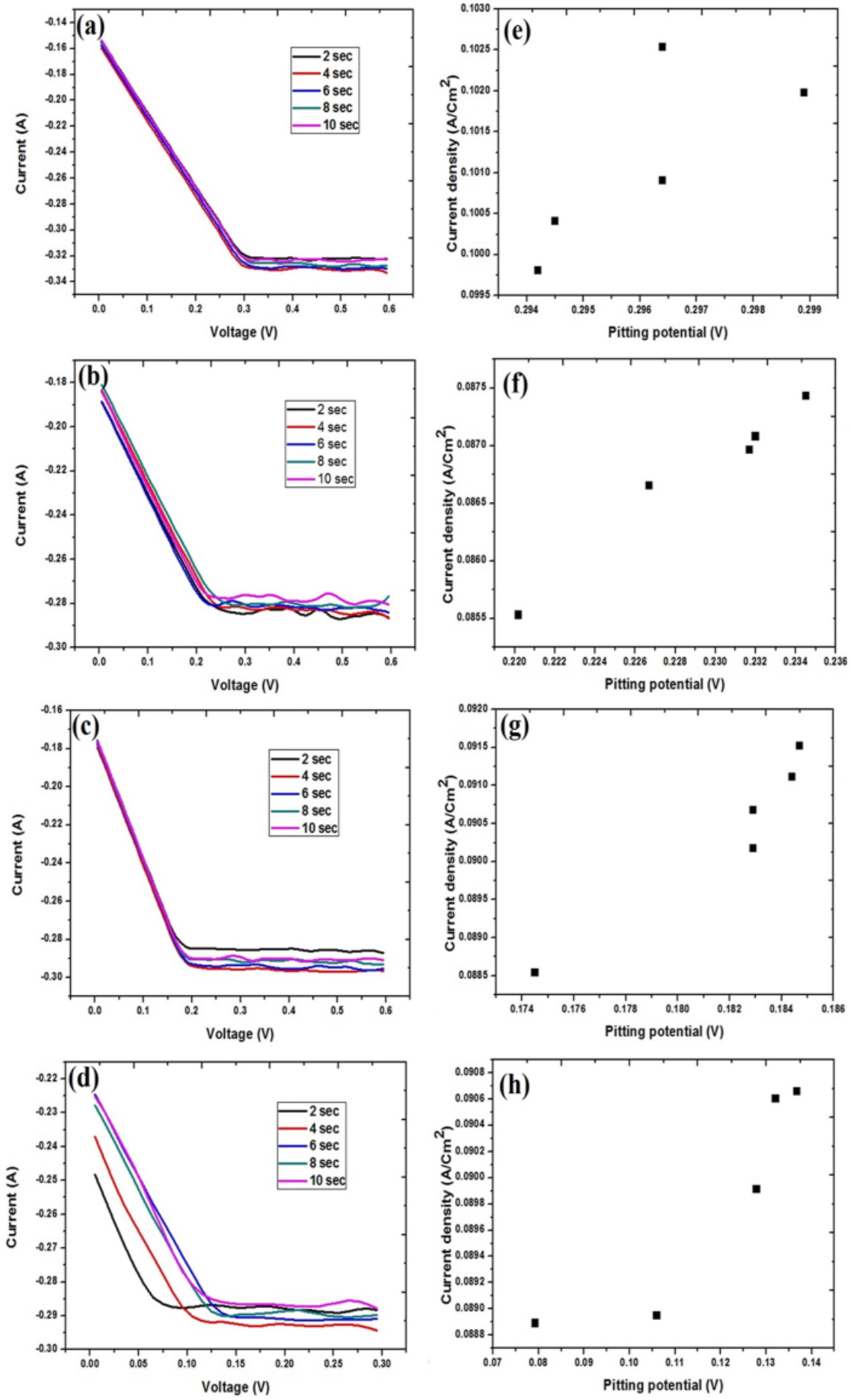

Fig. 8. Potentiometric curves and current density vs. pitting potential graphs of (a)(e) Yttria dispersed duplex stainless steel, (b)(f) Yttria dispersed ferritic stainless steel, (c)(g) duplex stainless steel, (d)(h) ferritic stainless steel respectively at 0.5 M H_2SO_4 solution

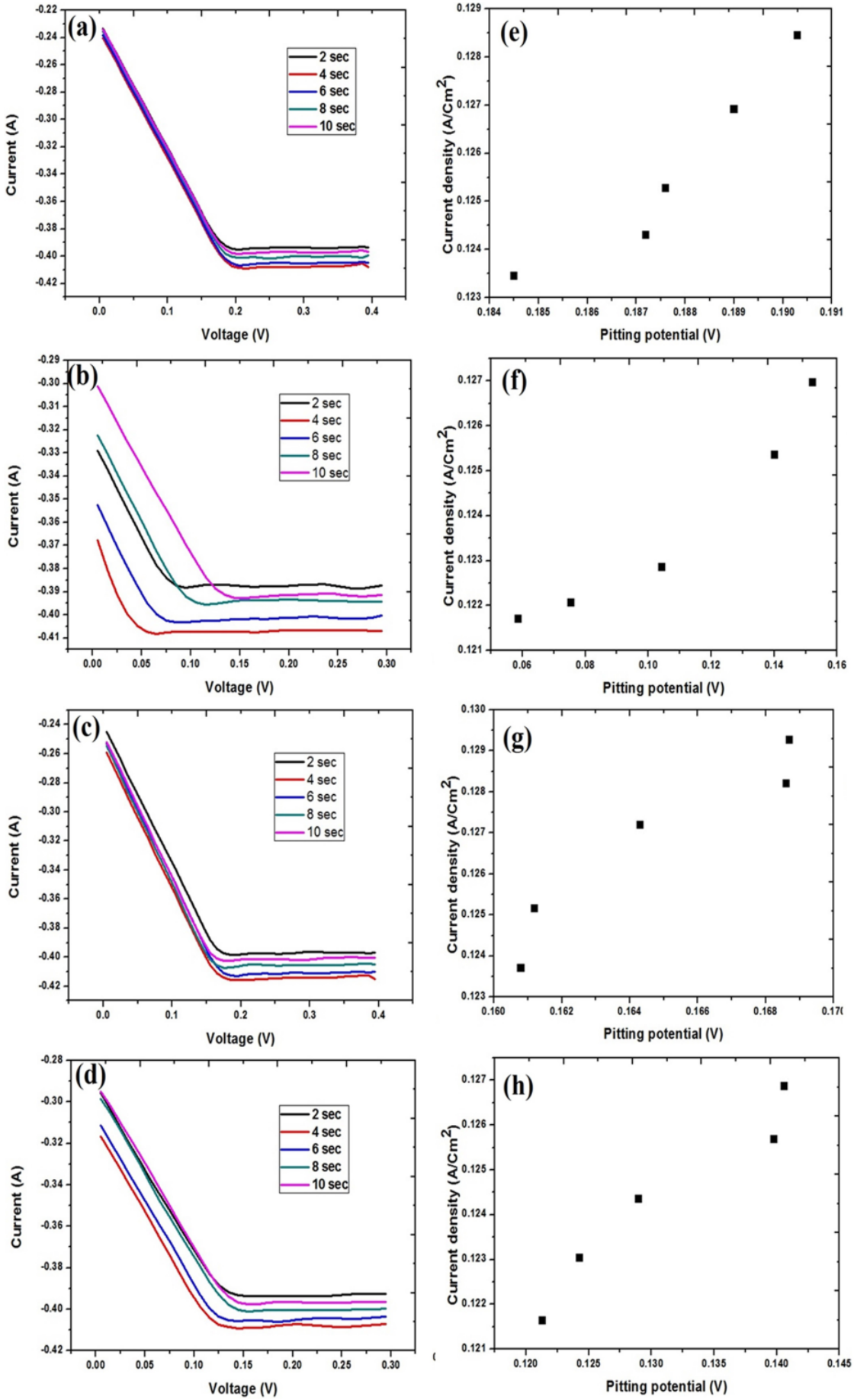

Fig. 9. Potentiometric curves and current density vs. pitting potential graphs of (a)(e) Yttria dispersed duplex stainless steel, (b)(f) Yttria dispersed ferritic stainless steel, (c)(g) duplex stainless steel, (d)(h) ferritic stainless steel respectively at 1 M H_2SO_4 solution

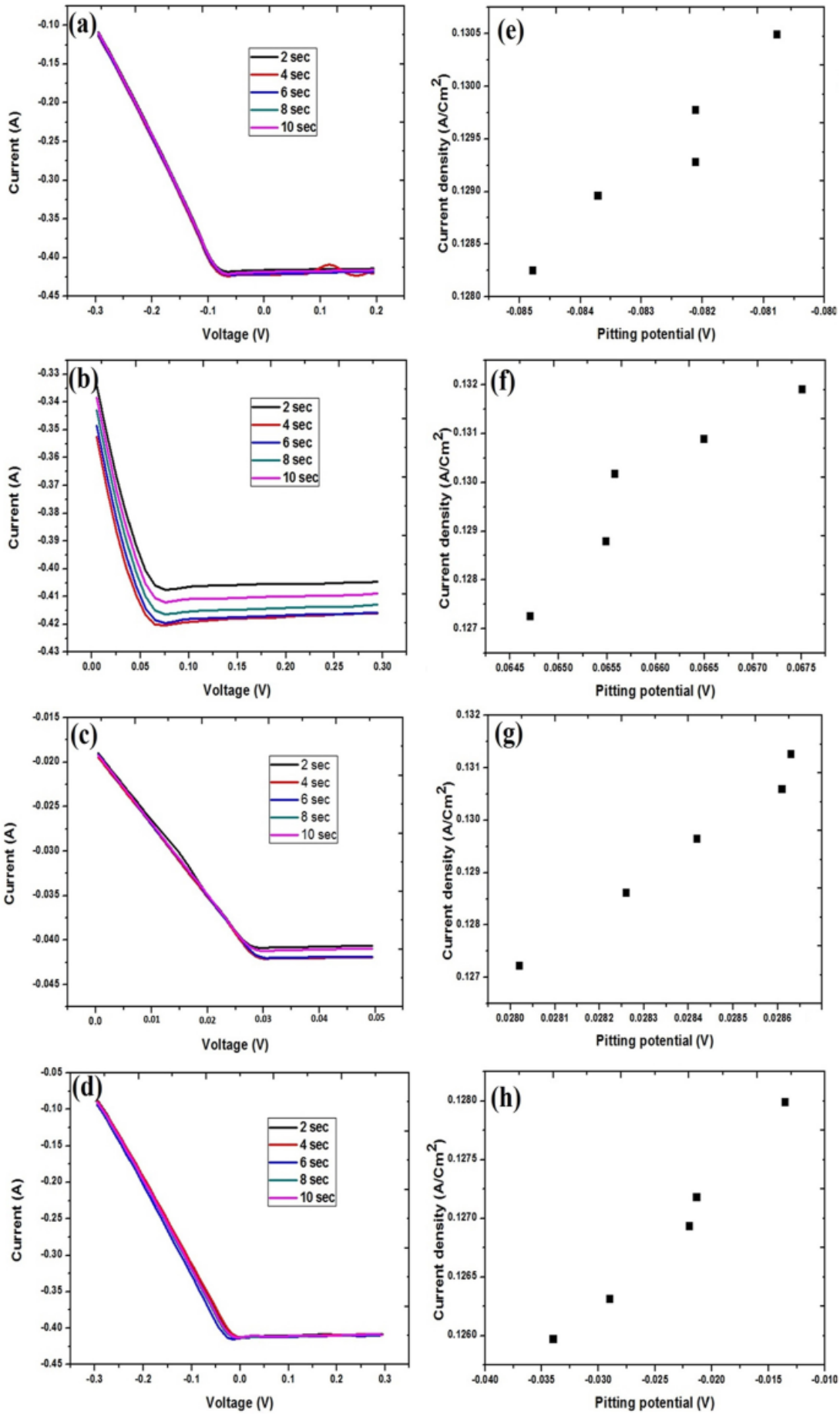

Fig. 10. Potentiometric curves and current density vs. pitting potential graphs of (a)(e) Yttria dispersed duplex stainless steel, (b)(f) Yttria dispersed ferritic stainless steel, (c)(g) duplex stainless steel, (d)(h) ferritic stainless steel respectively at 2 M H_2SO_4 solution

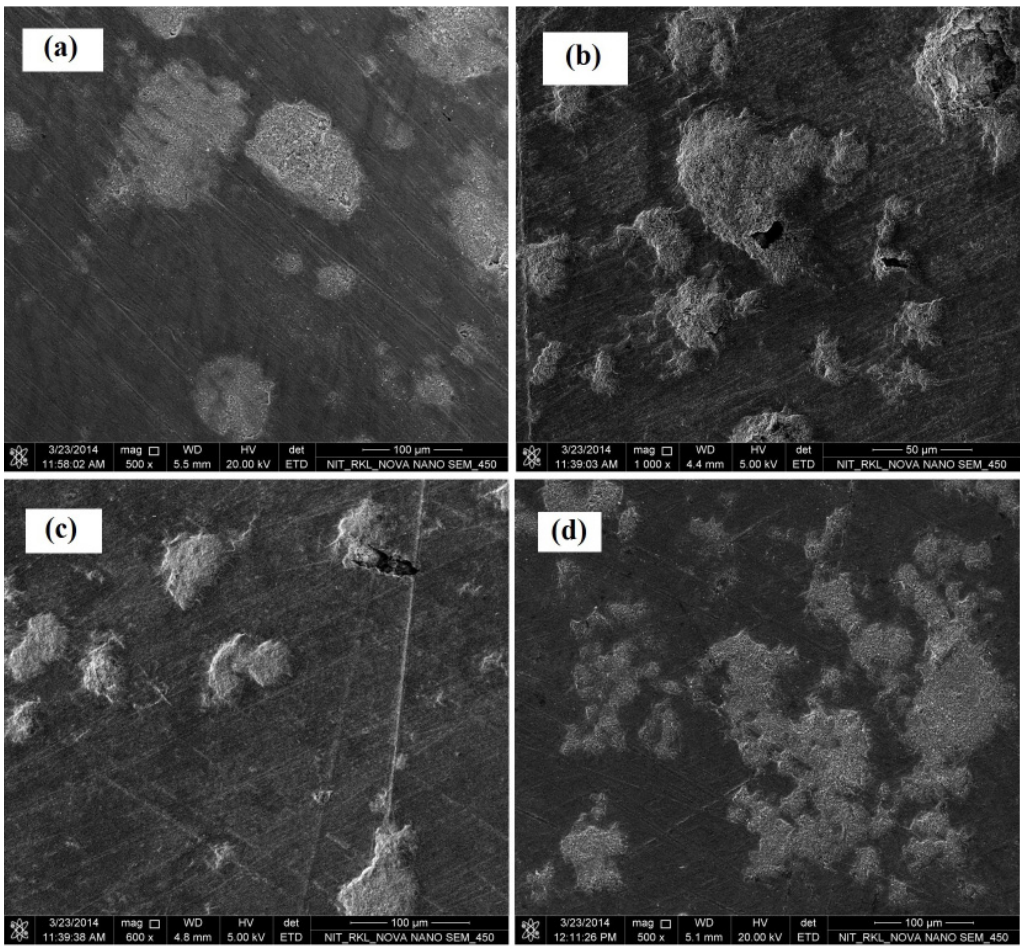

Fig. 11. FESEM images of (a) Yttria dispersed duplex stainless steel (b) Yttria dispersed ferritic stainless steel (c) duplex stainless steel (d) ferritic stainless steel

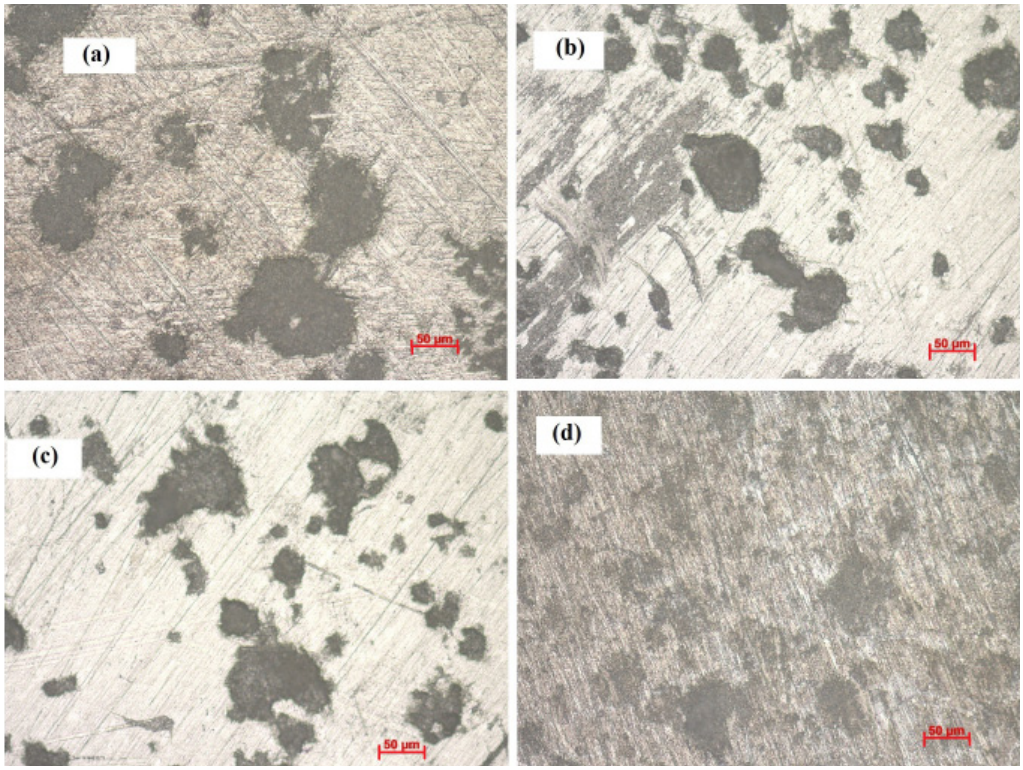

Fig. 12. Optical microstructure study of (a) Yttria dispersed duplex stainless steel (b) Yttria dispersed ferritic stainless steel (c) duplex stainless steel (d) ferritic stainless steel

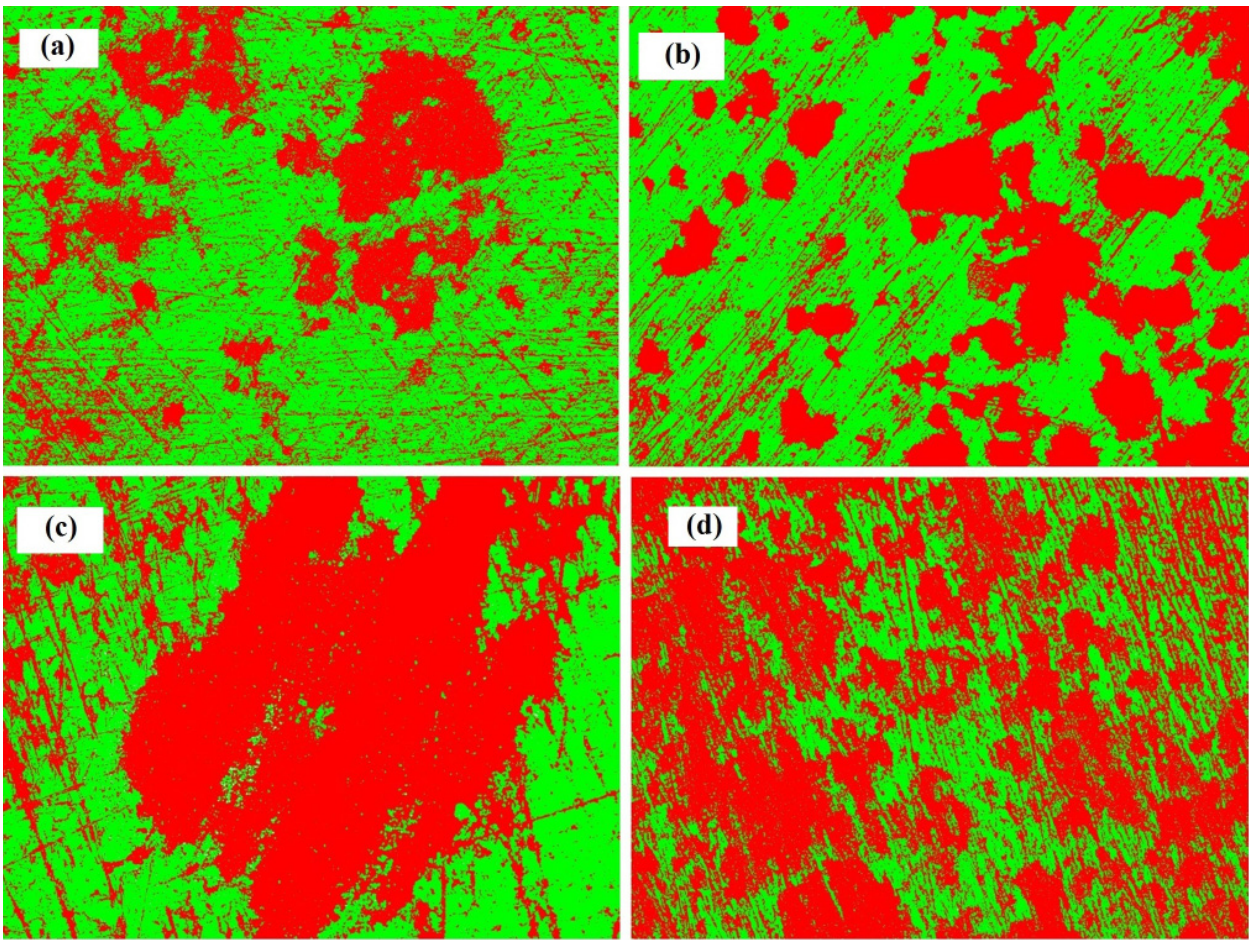

Fig. 13. Optical phase analysis of (a) Yttria dispersed duplex stainless steel (b) Yttria dispersed ferritic stainless steel (c) duplex stainless steel (d) ferritic stainless steel using Axio Vision Release software. (Similar to Fig. 12, all the images of Fig. 13 are in a magnification of 50 μm scale bars)

red colour region corresponds to corroded (iron oxide) stainless steel part and green colour corresponds to unaffected stainless steel. There is a gradual increase in the corrosion from yttria dispersed stainless steel to yttria free stainless steel samples.

TABLE 1

The values of E_P, I_P in NaCl and H_2SO_4 electrolytes at different concentrations

Condition	Type of stainless steel	Volume fraction of Fe_2O_3	Concentration (M)	NaCl		H_2SO_4	
				E_P (V)	J (mA/cm^2)	E_P (V)	J (mA/cm^2)
Yittria dispersed stainless steel	Duplex stainless steel	37	0.5	1.45	16.46	0.30	102.54
			1	0.67	47.81	0.19	128.45
			2	0.63	66.64	–0.08	130.50
	Ferritic stainless steel	42	0.5	0.64	13.92	0.23	87.43
			1	0.43	41.22	0.15	126.97
			2	0.42	38.91	0.06	131.90
Yittria free stainless steel	Duplex stainless steel	61	0.5	0.63	60.02	0.18	91.52
			1	0.57	41.33	0.16	129.26
			2	0.24	64.56	0.02	131.25
	Ferritic stainless steel	64	0.5	0.57	86.45	0.14	90.66
			1	0.19	35.33	0.14	126.87
			2	0.18	17.52	–0.01	128.0

5. Conclusions

Mechanically alloyed duplex and ferritic stainless steel samples dispersed with yttria and without yttria were consolidated by SPS method at a load of 50 MPa and 1000°C temperature under vacuum for 5 minutes. XRD and microstructural analysis were performed for consolidated stainless steel samples before corrosion study. From XRD it is confirmed that yttria acts as austenitic stabilizer but more research should be conducted to study the actual role of yttria as austenitic stabilizing agent. We successfully studied the corrosion properties of consolidated stainless steel samples by LSV method at different concentration of NaCl and H_2SO_4 solutions. As the concentration of NaCl and H_2SO_4 electrolytes increases from 0.5 to 2.0 M then pitting potential for all the four stainless steel samples decreases due to the accelerated rate of corrosion reactions at higher concentrations. In case of NaCl, E_P decreases with increasing current density but in case of H_2SO_4, E_P increases with increasing current density due to the formation of $FeSO_4$ protective layer along with Cr_2O_3 layer. At 0.5 M NaCl, pitting potential (E_P) of yttria dispersed duplex and ferritic stainless steel samples are found to be 1.45 V and 0.64 V and that of yttria free duplex and ferritic stainless steel samples show E_P value of 0.63 V and 0.57 V. Similarly E_P value

of yttria dispersed duplex and ferritic stainless steel samples at 0.5M H_2SO_4 are 0.30 V and 0.23 V respectively and that of yttria free duplex and ferritic stainless steel samples show E_P value of 0.18 V and 0.14 V. Microstructural analysis by FESEM and optical microscope show corroded regions of stainless steel samples. Volume fraction of iron oxide (corrosion) present in yttria dispersed duplex and ferritic stainless steel samples are 37 and 42% respectively and that of yttria free duplex and ferritic stainless steel samples are 61 and 64% respectively.

Acknowledgement

Financial support for this work from the Council of Scientific & Industrial Research (CSIR), India (Grant No. 22/561/11/EMR II Dated 11.04.2011) is gratefully acknowledged. The authors are also grateful to Dr. D. Chakravarty, ARCI Hyderabad, India for providing SPS facility.

REFERENCES

[1] R. Shashanka, D. Chaira, B.E. Kumara Swamy, Int. J. Electrochem. Sci. **10**, 5586-5598 (2015).
[2] Tuba Karahan, Hayriye Ertek Emre, Mustafa Tumer, Ramazan Kacar, Mater. Des. 55, 250-256 (2014).
[3] R. Shashanka, D. Chaira, Powder Technol. **278**, 35-45 (2015).
[4] R. Shashanka, D. Chaira, Mater Charact. **99**, 220-229 (2015).
[5] J. Shankar, A. Upadhyaya, R. Balasubramaniam, Corros. Sci. **46**, 487-498 (2004).
[6] R.M. German, Sintering Theory and Practice, Wiley-Interscience Publications, New York, 1996.
[7] S.K. Mukherjee, G.S. Upadhyaya, Int. J. Powder Metall. Powder Tech. **19**, 289 (1983).
[8] S.K. Mukherjee, G.S. Upadhyaya, J. Powder Bulk Solid Tech. **7**, 27 (1983).
[9] K. Dash, D. Chaira, B.C. Ray, Mater. Res. Bull. **48**, 2535-2542 (2013).
[10] Kyoung Hun Kim, Jae Hong Chae, Joo Seok Park, Jong Pil Ahn, Kwang Bo Shim, J. Ceram Process Res. **10**, 716-720 (2009).
[11] M. Tokita, J. Soc. Powder Tech. Jpn. **30**, 790-804 (1993).
[12] M. Omori, Mater. Sci. Eng. A. 287, 183-188 (2000).
[13] K.H. Kim, K.B. Shim, Mater. Character. **50**, 31-37 (2003).
[14] S. Balaji, A. Upadhyaya, Mater Chem Phys. **101**, 310-316 (2007).
[15] R. Liu, D.Y. Li, J. Mater Sci. **35**, 633-641 (2000).
[16] E.J. Felten, J. Electrochem. Soc. 108, 490-495 (1961).
[17] C.S. Wukusick, J.F. Collins, Mat. Res. Standard. **4**, 637-646 (1964).
[18] J.M. Francis, W. H. Whitlow, Corros. Sci. **5**, 701-710 (1965).
[19] S. Lal, G.S. Upadhyaya, Rev. Powder Metall. Phys. Ceram. **3**, 165-203 (1986).
[20] S. Lal, G.S. Upadhyaya, J. Mater. Sci. Lett. **6**, 761-764 (1987).
[21] S. Ningshen, M. Sakairi, K. Suzuki, S. Ukai, Corros. Sci. **78**, 322-334 (2014).
[22] Jian Chen, R. Matthew Asmussen, Dmitrij Zagidulin, James J. Noel, David W. Shoesmith, Corros. Sci. **66**, 142-152 (2013).
[23] C.X. Li, T. Bell, Corros. Sci. 48, 2036-2049 (2006).
[24] M. Metikos-Hukovic, R. Babic, Z. Grubac, Z. Petrovic, N. Lajci, Corros. Sci. **53**, 2176-2183 (2011).
[25] Basics of Voltammetry and Polarography, Princeton Applied Research, Applied Instruments Group, Application Note p-2.
[26] R. Shashanka, B.E. Kumara Swamy, S. Reddy, D. Chaira, Anal. Bioanal. Electrochem. **5**, 455-466 (2013).
[27] S. Reddy, B.E. Kumara Swamy, S. Aruna, M. Kumar, R. Shashanka, H. Jayadevappa, Chemical Sensors **7**, 1-8 (2012).
[28] V.K. Gupta, A. Nayak, S. Agarwal, B. Singhal, Combinatorial Chemistry & High Throughput Screening **14**, 284-302 (2011).
[29] R. Jain, V.K. Gupta, N. Jadon, K. Radhapyari, Analytical biochemistry **407**, 79-88 (2010).
[30] V.K. Gupta, A.K. Jain, G. Maheshwari, Talanta **72**, 1469-1473 (2007).
[31] R. Shashanka, D. Chaira, Powder Technol. **259**, 125-136 (2014).
[32] R. Shashanka, D. Chaira, B.E. Kumara Swamy, International Journal of Scientific & Engineering Research. **6**, 1863-1871 (2015).
[33] S. Gupta, R. Shashanka, D. Chaira, 4th National Conference on Processing and Characterization of Materials, IOP Conf. Series: Materials Science and Engineering **75**, 012033 (2015).
[34] R. Shashanka, D. Chaira, B.E. Kumara Swamy, International Journal of Scientific & Engineering Research. **7**, 1275-1285 (2016).
[35] A.K. Nayak, R. Shashanka, D. Chaira, IOP Conf. Series: Materials Science and Engineering 115 (2016) 012008. doi:10.1088/1757--899X/115/1/012008.
[36] R. Shashanka, D. Chaira, Acta Metallurgica Sinica (English Letters) **29**, 58-71 (2016).
[37] R. Shashanka, D. Chaira, D. Chakravarty, Journal of Materials Science and Engineering B **6**, 111-125 (2016).
[38] R. Shashanka, D. Chaira, Tribol. T. (2016) http://dx.doi.org/10.1080/10402004.2016.1168897.
[39] E. Blasco-Tamarit, D.M. García-Garcia, J. Garcia Anton, Corros. Sci. **53**, 784-795 (2011).
[40] Sulphuric Acid on the Web, Knowledge for the Sulphuric Acid Industry, Corrosion, June 6, (2005).